IEEE Access
Multidisciplinary | Rapid Review | Open Access Journal

Received 25 September 2023, accepted 12 November 2023, date of publication 20 November 2023,
date of current version 27 November 2023.

Digital Object Identifier 10.1109/ACCESS.2023.3334607

RESEARCH ARTICLE

Peak Demand Management and Voltage Regulation Using Coordinated Virtual Power Plant Controls

HARSHA PADULLAPARTI[1], (Senior Member, IEEE), ANNABELLE PRATT[1], (Senior Member, IEEE), ISMAEL MENDOZA[1], (Member, IEEE), SOUMYA TIWARI[1], (Member, IEEE), MURALI BAGGU[1], (Senior Member, IEEE), CHRIS BILBY[2], (Member, IEEE), AND YOUNG NGO[3], (Member, IEEE)

[1]National Renewable Energy Laboratory, Golden, CO 80401, USA
[2]Holy Cross Energy, Glenwood Springs, CO 81601, USA
[3]Survalent Technology Corporation, Brampton, ON L6Y 5X5, Canada

Corresponding author: Harsha Padullaparti (HarshaVardhana.Padullaparti@nrel.gov)

This work was authored in part by the National Renewable Energy Laboratory, operated by Alliance for Sustainable Energy, LLC, for the U.S. Department of Energy under Contract No. DE-AC36-08GO28308. Funding provided by U.S. Department of Energy Office of Electricity, Advanced Grid Research and Development Program.

ABSTRACT The aggregation of distributed energy resources (DERs) enables them to provide various grid services as a virtual power plant (VPP). Utilities use enterprise control solutions, such as advanced distribution management systems (ADMS) and distributed energy resource management systems (DERMS), to efficiently integrate DERs and realize the benefits of a VPP. These control solutions can complement each other to offer additional benefits. This paper evaluates the coordinated operation of an ADMS and a DERMS that collectively implements a VPP to provide peak demand reduction and voltage regulation through the simulation of an actual distribution feeder. A commercial ADMS reduces the peak demand through conservation voltage reduction (CVR). A prototype DERMS dispatches residential battery energy storage systems (BESS) based on real-time optimal power flow to provide additional peak demand reduction. The DERMS also maintains voltage regulation across the feeder by controlling both residential batteries and rooftop PV systems. The results from the controller-hardware-in-the-loop (CHIL) real-time simulations conducted in a realistic laboratory environment show that the coordinated operation of the ADMS and the DERMS effectively achieves peak demand reduction while enforcing voltage regulation across the feeder. Specifically, the ADMS dynamic voltage regulation (DVR) application and DERMS working together achieved a peak demand reduction of nearly 500 kW, whereas the ADMS DVR application alone obtained a reduction of approximately 100 kW. The DERMS VPP control in this work relies on the residential BESS for the demand reduction; the demand reduction accomplished depends on the BESS capacity available in the distribution system.

INDEX TERMS Advanced distribution management system (ADMS), DER aggregator, distributed energy resource (DER), distributed energy resource management system (DERMS), distribution system, energy storage, optimal power flow, virtual power plant (VPP), voltage regulation.

NOMENCLATURE

Acronyms

ADMS	Advanced distribution management system.
AMI	Advanced metering infrastructure.
ANSI	American National Standards Institute.
BESS	Battery energy storage system.
CHIL	Controller-hardware-in-the-loop.
CVR	Conservation voltage reduction.
DER	Distributed energy resource.
DERMS	Distributed energy resource management system.

The associate editor coordinating the review of this manuscript and approving it for publication was Fabio Massaro.

DNP3	Distributed Network Protocol 3.
DVR	Dynamic voltage regulation.
EMT	Electromagnetic transient.
EPRI	Electric Power Research Institute.
EV	Electric vehicle.
HCE	Holy Cross Energy.
HELICS	Hierarchical Engine for Large-scale Infrastructure Co-Simulation.
LTC	Load tap changer.
NREL	National Renewable Energy Laboratory.
NRECA	National Rural Electric Cooperative Association.
NSRDB	National solar Radiation Database.
p.u.	Per unit.
PV	Photovoltaic.
RT-OPF	Real-time optimal power flow.
SCADA	Supervisory control and data acquisition system.
SOC	State of charge.
VPP	Virtual power plant.
VR	Voltage regulator.
ZIP	Constant impedance, Z, constant current, I, and constant power, P.
Metrics	
PR_{max}	Maximum substation demand reduction (kW).
T_{ex}	Total duration of voltage exceedances (node-hours).
Q_{max}	Maximum PV reactive power output (kvar).
N_t	LTC and VR tap changes.
ES	Energy savings (%).
Parameters	
Avg. V	Average voltage (p.u.).
Avg. SOC	Average state of charge (%).
P_a, P_b, P_c	Substation active power demands in phases A, B, C (kW).
P_{PV}	Total active power output from PV (kW).
Q_{PV}	Total reactive power output from PV (kvar).
P_{BESS}	Total active power output from BESS (kW).

I. INTRODUCTION

More than 200 million distributed energy resources (DERs)—such as photovoltaic systems (PV), battery energy storage systems (BESS), electric vehicles (EVs), and wind turbines—are expected to be integrated into distribution grids by 2030 [1]. This constitutes nearly 200 GW of flexible load within the United States alone, which represents 20% of the forecasted peak demand [2]. DERs can create several operational challenges, including voltage issues, overloading, reverse power flows, and protection miscoordination [3], [4]. To ensure the secure, reliable, and efficient operation of distribution networks, utilities are increasingly deploying intelligent controls, such as advanced distribution management systems (ADMS) [5] and distributed energy resource management systems (DERMS) [6].

An ADMS is an integrated platform that provides the distribution system operator with various network monitoring, analysis, and control functions—such as volt/VAR optimization, fault management, and outage management—for optimized grid operation [5]. The ADMS receives the real-time measurement data from numerous points across the distribution network via the supervisory control and data acquisition (SCADA) system; however, the ADMS typically does not have visibility of or control over the behind-the-meter DER assets [1]. On the other hand, the DERMS solutions are focused on monitoring and controlling the decentralized DERs, including the behind-the-meter residential PV and BESS [7]. The DERMS can optimize and dispatch the DERs to support various grid services, such as peak load management, voltage regulation, congestion management, and demand response [8], [9].

When the DERMS operations are coordinated with the ADMS, the DERMS can offer additional services in the form of a virtual power plant (VPP). A VPP refers to the aggregation of DERs to form a single larger power plant [10]. The ability to monitor and control the DERs—both the utility-scale and behind-the-meter DERs—in distribution grids is key to realizing a VPP. This paper evaluates the coordinated operation of a commercial ADMS and a prototype DERMS in achieving peak load reduction and voltage regulation.

Several works in the literature focus on controlling DER groups—such as flexible residential loads [11], [12] and commercial building loads [13]—to follow power reference set points at the substation. The works [14], [15], [16], [17] involved the aggregation of various DER groups to provide grid services, such as peak load management, flexibility, and frequency regulation. Many recent studies developed solutions for aggregating EVs [18], [19], [20], [21] to support grid benefits. All these works, however, ignore the network power flows and the associated constraints. As a result, the bus voltage levels are not guaranteed to stay within the American National Standards Institute (ANSI) voltage limits [22]. Voltage control methods using feedback-based real-time optimization can be used to ensure voltage regulation. These methods use network information and real-time measurements to dispatch the DERs. The methods using the voltage measurement feedback [23], [24], distributed control strategies [25], [26], [27], [28], [29], and manifold-based algorithms [30], [31], [32] are some examples that enforce voltage regulation in distribution networks, but they do not include VPP controls.

Most of the aforementioned works use numerical simulations of small test systems and do not study coordination with existing enterprise controls at the utility, such as an ADMS. For the practical applicability of these technologies, it is important to evaluate their performance with actual distribution feeder models and hardware controllers to study the potential challenges related to scalability, system integration, and instability. The findings from such realistic studies can help utilities derisk deployment in the field.

Further, although the integration of ADMS and DERMS is a desirable industry progression [1], [7], [33], [34], the relevant studies are lacking; the works reported in this regard [35], [36], [37], [38] demonstrate only voltage regulation using the ADMS-DERMS coordination. To address these gaps, this paper evaluates the performance of the coordinated ADMS-DERMS operation in achieving peak load reduction using residential PV smart inverters and BESS while maintaining voltage regulation. A commercial ADMS is interfaced with a prototype DERMS using industry-standard protocols for this evaluation. The ADMS reduces the peak demand using a dynamic voltage regulation (DVR) application [39]. The DVR application controls legacy assets, such as load tap changers (LTCs) and voltage regulators (VRs), to reduce the system voltages. As a result, the load demand is reduced through conservation voltage reduction (CVR). CVR is a process of reducing the load demand by reducing the bus voltages. The real-time optimal power flow (RT-OPF) algorithm, developed in [40], which uses network information and voltage and power measurement feedback for the VPP and voltage regulation controls, is used for the prototype DERMS. The linearized power flow approximation methodology of [40], which is employed in this study, can be applied to multi-phase distribution networks with both radial and meshed topologies. This paper studies the individual contributions of the ADMS and prototype DERMS solutions as well as their contribution when interfaced with each other in achieving peak demand reduction and voltage regulation. Specifically, we demonstrate that their coordinated operation offers superior performance compared to when they are acting alone.

The key contributions of this paper are to:

1. Evaluate the performance of ADMS and DERMS using a real-world distribution feeder. We interface a commercial ADMS with a prototype DERMS and use a detailed feeder model developed using the data provided by a utility for the evaluation.

2. Provide insights into the coordinated operation of the ADMS and DERMS in achieving peak demand reduction and voltage regulation compared to each control acting independently.

3. Offer guidance to distribution utilities on the field deployment of ADMS and DERMS solutions and the expected benefits. This helps the utilities in making investment decisions.

In the remainder of this paper, Section II includes the distribution system modeling details. Section III presents the real-time simulation setup, the ADMS-DERMS integration, and the cosimulation details. Section IV describes the metrics used for the evaluation. Section V discusses the simulation scenarios and results. Finally, Section VI provides the conclusions.

II. DISTRIBUTION FEEDER MODELING

A detailed distribution feeder model developed based on the data from the utility Holy Cross Energy (HCE) is used for the demonstrations in this study. This is a 14.4-kV feeder with a peak load of 4.5 MW, located in Colorado within the service territory of the utility. The topology of the feeder is shown in Fig. 1. The legacy devices on this feeder for voltage regulation include a load tap changer (LTC) at the substation and three single-phase VRs installed at a three-phase bus, as highlighted in Fig. 1. There are 1,137 residential loads modeled, of which 163 loads represent all-electric homes. We assumed that these homes have PV and BESS installed on their premises that participate in the VPP and voltage regulation controls by the DERMS. The voltage feedback locations for the DVR application of the ADMS, described in Section III-A, as well as the all-electric homes with DERs where the DERMS receive the voltage measurement feedback, are marked in Fig. 1.

In the United States, high load demand in power distribution systems is typically observed during the late afternoon and early evening hours. This time period is often referred to as the ''peak demand'' or ''peak load'' hours. It typically occurs between 4:00 p.m. and 8:00 p.m., when businesses are still operating at the same time that many people are returning home from work, and household energy consumption increases as people cook dinner, use appliances, and engage in other activities that require electricity. The exact timing can vary depending on geographic location, climate, and local energy consumption patterns. In the area where Holy Cross Energy's distribution feeder is located, the peak demand occurs between 4 p.m. and 9 p.m. [41]. We selected the time frame from 4:30-7:30 p.m. because it falls within the anticipated peak demand window, and it represents high load demand with low PV generation conditions, making it suitable for peak demand management studies. This is an ideal period to perform peak demand reduction to reduce the demand charges. Therefore, we selected the simulation period 4:30 p.m.-7:30 p.m. on December 30, 2019, for the real-time simulations because this period has high load demand and low PV generation, making it an ideal period to perform peak demand reduction to reduce the demand charges.

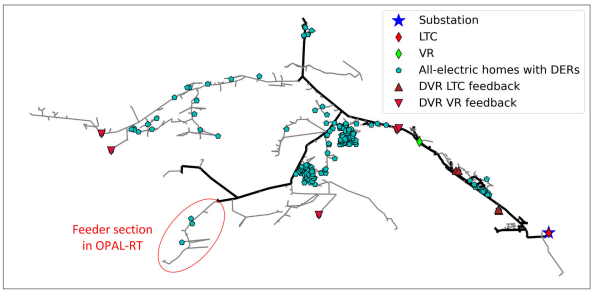

FIGURE 1. Topology of the distribution feeder.

The loads are modeled as ZIP loads to account for the voltage dependency. The ZIP coefficients [0.24, 0.36, 0.4] are selected based on [42] and a pilot study conducted by another utility and are used for the load modeling. Further, the time-varying load profiles generated based on the actual advanced metering infrastructure (AMI) data collected in the

field are used for the loads. Solar irradiance data pertaining to the feeder location were downloaded for the full year from the National Solar Radiation Database (NSRDB) [43]. These data are used as inputs to all the PV systems. The PV profile for the simulated day is shown in Fig. 2; the profile during the simulation period is highlighted in red.

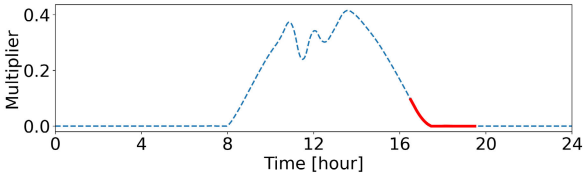

FIGURE 2. Solar irradiance profile.

The PV and BESS are modeled using the standard PV system and storage objects available in OpenDSS. The PV panel is sized such that the total annual generation matches 120% of the total annual load consumption at the same residential location [44]. Additionally, the PV inverter kVA rating is assumed to be 110% of its kW rating. The BESS sizes are assumed such that their peak kW values are higher than those of the PV units considering the discrete sizes of commercially available BESS products. Additionally, the BESS capacity ratings are selected based on the commercially available products for these kW ratings of the BESS. Further, the initial BESS state of charge (SOC) at the beginning of the simulation period is set at 80%, and the lower SOC limit below which the BESS would stop discharging is set at 20%. The total residential PV and BESS ratings are shown in Table 1. The PV penetration level is 35% relative to the peak load.

TABLE 1. Total residential PV and BESS ratings.

DER	Phase A	Phase B	Phase C	Total
PV power	495 kW	588 kW	552 kW	1635 kW
BESS power	295 kW	360 kW	335 kW	990 kW
BESS capacity	796 kWh	972 kWh	904 kWh	2372 kWh

III. REAL-TIME SIMULATION SETUP FOR VIRTUAL POWER PLANT AND VOLTAGE REGULATION EVALUATION

This paper demonstrates the coordinated operation of an ADMS and a DERMS, which operates a VPP, in achieving peak load reduction and voltage regulation on a national, vendor-neutral ADMS test bed. The ADMS test bed was developed at the National Renewable Energy Laboratory (NREL) with funding from the U.S. Department of Energy Office of Electricity to enable utilities, vendors, and researchers to evaluate existing and future ADMS, DERMS, and other utility management system applications as well as grid control architectures in a realistic laboratory environment [45].

The real-time simulation setup used in this work is shown in Fig. 3. The ADMS test bed consists of multiple subsystems, including a multi-timescale simulation platform and hardware controllers. It also includes a prototype DERMS developed at NREL. A commercial ADMS, SurvalentONE, is interfaced with the simulation and hardware components of the test bed using industry-standard communications protocols. The MultiSpeak communications standard is used to interface the ADMS and the DERMS. The details of the individual subsystems and their integration are presented in this section.

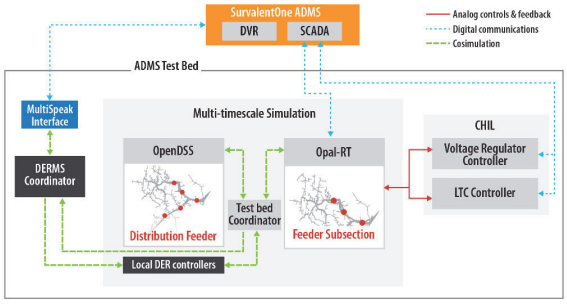

FIGURE 3. Schematic of the ADMS test bed for the VPP evaluation.

A. ADMS AND DVR

We used SurvalentONE's DVR application for the feeder demand reduction. For this evaluation, the ADMS had control of an LTC at the substation and a VR halfway downstream of the feeder, as shown in Fig. 1. The laboratory setup included the substation LTC to help illustrate the impact of the DVR in the entire feeder, even though HCE does not have control of the substation control equipment; HCE's bulk electricity provider has control of the substation equipment in the field. The initial voltage set point and the limit for each device are listed in Table 2. Additionally, the LTC and VR local controllers use a deadband of 3 V and 2 V around their voltage set points, respectively. The DVR application relies on SCADA data or AMI information to avoid exceeding any voltage restrictions or operational limits. During our testing, the DVR execution was configured to evaluate the feeder status every minute and issue a new set point to help quickly obtain energy savings. This was made possible by setting the SCADA to a polling cycle of 30 seconds. There are six voltages used for feedback—three for the LTC and three for the VR—to allow the DVR application to correct or control the voltage along the feeder. Three points are selected to be near the device, and the other three are selected to represent voltages far from each controller. These six locations are marked in Fig. 1.

TABLE 2. LTC and VR set points and limits.

Regulator	Initial Set Point	Near High Limit	Near Low Limit	Far High Limit	Far Low Limit
LTC	121 V	124 V	115 V	124 V	114 V
VR	123 V	124 V	115 V	124 V	114 V

The ADMS also issues a feeder head power limit for the DERMS to maintain by using its VPP controls.

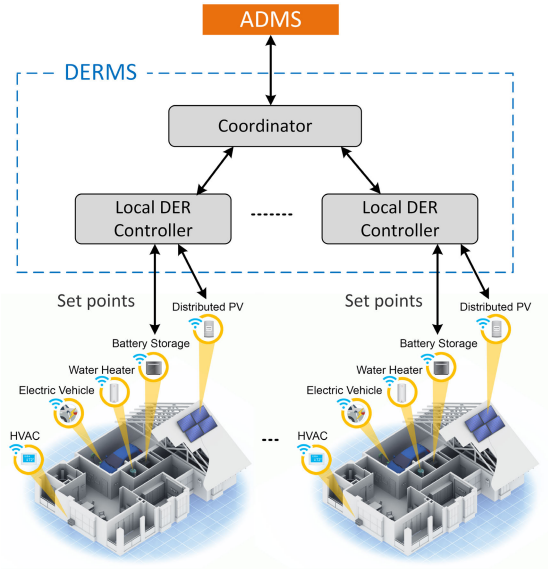

FIGURE 4. Illustration of prototype DERMS.

B. PROTOTYPE DERMS

The prototype DERMS developed at NREL [46], [47], based on the RT-OPF algorithm proposed in [40], is used in this work. The DERMS comprises a coordinator and a set of local DER controllers, as illustrated in Fig. 4. For this real-time simulation setup, only the PV and BESS are controlled, but the DERMS can also manage EVs; electric water heaters; and heating, ventilating, and air-conditioning systems. The coordinator receives the feeder head power measurements and bus voltage measurements from the all-electric home locations across the feeder in real-time as feedback. Other voltage locations could be added, as needed. Also, in this real-time simulation setup, these data are provided by the test bed coordinator (described in Section III-E) from OpenDSS and OPAL-RT, but in the field, the feeder head data would come from ADMS SCADA and the bus voltage from local DER controllers, and this was demonstrated with the test bed in [37]. Then it computes the dual variables (gradients) for each local DER controller. These gradient signals are then communicated to the individual local DER controllers.

Each local DER controller uses the gradients received from the coordinator and the DER statuses, such as power outputs from the PV and BESS SOC to solve the optimal set points for different DERs associated with that local DER controller. These set points are then sent to the individual DERs. This computation happens during each simulation time step, and the DER power outputs are updated accordingly in real-time. The collective response of all the local DER controllers ensures that the system-wide objectives are met. Specifically, active power tracking at the feeder head is ensured when the DERMS VPP control is enabled, and the bus voltage regulation across the feeder is ensured when the DERMS voltage regulation is enabled.

C. MULTI-TIMESCALE SIMULATION

The ADMS test bed used for the real-time simulations is shown in Fig. 5. The ADMS test bed runs a real-time, multi-timescale simulation of the distribution feeder, including any DERs, in OpenDSS and OPAL-RT's electromagnetic transient (EMT) simulation tool. Most of the feeder is simulated in OpenDSS, a quasi-static time-series simulator with a time step resolution of 2 s. The remaining section, which is referred to as the "subtree" and is encircled in Fig. 1, consists of 70 nodes and is simulated using OPAL-RT's EMT simulation tool, eMEGASIM, at a simulation time step of 100 μs. OPAL-RT is a digital real-time simulator to which the LTC and VR hardware controllers are interfaced. The subtree feeder head in OPAL-RT is modeled as a Thevenin circuit. The Thevenin impedance is calculated based on the short-circuit impedance at the point of common coupling. During the multi-timescale simulation, the subtree head voltage magnitude and angle are received from OpenDSS, and the active and reactive power at the subtree head are fed back from eMEGASIM to OpenDSS to close the power flow loop [37].

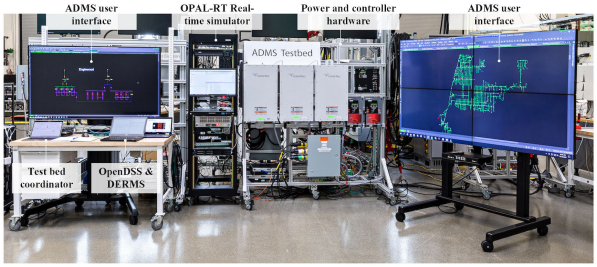

FIGURE 5. ADMS test bed used for real-time simulations.

D. HARDWARE CONTROLLERS

The LTC and VR hardware controllers are interfaced with the simulation through OPAL-RT to perform controller-hardware-in-the-loop (CHIL) cosimulations. The Beckwith Electric LTC and a Schweitzer Engineering Laboratories VR controller were configured per the field settings. The analog interfaces of the OPAL-RT platform provided the simulation input necessary to incorporate the LTC and VR controllers as CHIL. Distributed Network Protocol 3 (DNP3) communications between the SurvalentONE and both the LTC and VR were configured to provide situational awareness during the simulation. Additionally, this mode of communication allowed the ADMS to control both devices.

Once the DVR is enabled, the ADMS evaluates the current state of the feeder voltages and can issue a command to raise or lower the taps on the LTC and/or the VR controllers to achieve its objective. During the evaluation, to incorporate the control action of the hardware, the controllers provided an analog signal to the OPAL-RT during a tap operation that was digitized and communicated to the OpenDSS simulation. The controllers continue to issue a signal to raise or lower the tap position to the corresponding device in the OpenDSS

simulation until the feedback input to the controller reaches its set point operating band.

E. SUBSYSTEM INTEGRATION AND COSIMULATION

Besides the controller hardware, the subsystem integration efforts primarily focused on developing the industry-standard communications interfaces to interface the SurvalentONE ADMS with the DERMS and on developing a cosimulation manager referred to as the test bed coordinator.

The DERMS is interfaced with the ADMS using the MultiSpeak communications standard to enable coordinated operation. MultiSpeak [48] is a key industry-wide standard for enabling the interoperability of enterprise applications including ADMS and DERMS. It is most widely used by distribution utilities in the United States. We worked with the National Rural Electric Cooperative Association (NRECA), the developer of the MultiSpeak standard, to develop a business process to support the messages between the ADMS and DERMS for coordination.

The ADMS sends enable/disable commands to the DERMS as MultiSpeak messages for both VPP and voltage regulation controls. Additionally, the ADMS sends the target feeder head power references for the DERMS to track for the VPP control as well as the start time and the duration of the control event. NRECA provided a limited release of this new business process for our use, and Survalent updated its MultiSpeak interface to support this new process. We also partnered with the Electric Power Research Institute (EPRI) to provide a MultiSpeak interface for NREL's prototype DERMS.

Further, the OPAL-RT platform also has capabilities to communicate using industrial communications protocols, including DNP3 and Modbus. We used OPAL-RT's DNP3 communications interface to provide the voltage feedback from both eMEGASIM and OpenDSS to the ADMS.

The test bed coordinator, which is essentially a cosimulation manager developed in Python, is used to perform the cosimulations. The test bed coordinator uses the Hierarchical Engine for Large-scale Infrastructure Co-Simulation (HELICS) framework [49], a scalable, open-source platform that allows synchronous data exchange among multiple subsystems to perform integrated cosimulations through time. The test bed coordinator is responsible for enabling/disabling the DERMS VPP and voltage regulation functions in response to the commands received from the ADMS; setting the simulated device statuses in the OpenDSS using the Python library [50], including the LTC and VR tap positions, based on the signals received from the hardware controllers via OPAL-RT; and setting the PV and BESS simulated device powers based on the set points received from the DERMS. Further, it also collects the necessary measurement feedback data from the OpenDSS power flow and communicates these to the ADMS and the DERMS. Specifically, the feeder head power measurements and all-electric home bus voltages are communicated to the DERMS, and the feedback bus voltages for the DVR are communicated to the ADMS DVR controls at each time step.

IV. METRICS FOR EVALUATION

The performance of the coordinated operation of the ADMS and the DERMS in performing the VPP and voltage regulation controls is evaluated using the following metrics:

1. *Maximum substation demand reduction (PR_{max}):* This is the maximum active power demand reduction at the substation compared to the baseline during the simulation period.
2. *Total duration of voltage exceedances (T_{ex}):* The voltage magnitude of a bus being outside of the ANSI voltage range from 0.95 p.u.-1.05 p.u. is referred to as the voltage exceedance in this work. Further, a bus can have multiple phases, and each phase is considered as a node; thus, a three-phase bus has three nodes, and a single-phase bus has one node. The number of nodes exceeding the ANSI limits is multiplied by the duration of the exceedances and presented in the units of node-hours.
3. *Maximum PV reactive power output (Q_{max}):* The DERMS primarily relies on the reactive power support from the PV smart inverters to maintain the bus voltages within the limits. The maximum total PV reactive power output during the simulation period is recorded.
4. *LTC and VR tap changes (N_t):* The number of times the LTC and VR tap positions changed during the simulation period.
5. *Energy savings (ES):* The energy delivered by the substation in the baseline is computed first. Then the reduction in the energy delivered by the substation in the other scenarios is computed and expressed as a percentage of the energy delivered in the baseline. Note that the energy savings computed for the scenarios involving the BESS also include the energy supply from the BESS.

V. RESULTS AND DISCUSSION

The ability of the ADMS, in coordination with the DERMS, to deliver grid services is evaluated using five scenarios, as summarized in Table 3. The DVR and/or DERMS functionalities enabled/disabled in each scenario are also specified. For example, in the baseline scenario, both the DVR and DERMS are disabled. The LTC and VRs are operated by their local controllers using the initial set points in Table 2 in this scenario. In the DVR-only scenario, the DVR is enabled to control the LTC and the VR taps to reduce the demand through CVR, and the DERMS is disabled. Other scenarios follow along the same lines as specified in Table 3. The times when the DVR, DERMS VPP, and DERMS voltage regulation controls are enabled/disabled in the scenarios wherever applicable are fixed and listed in Table 4. They are also marked in the figures by the vertical dashed black lines.

TABLE 3. Real-time simulation scenarios.

Scenario	DVR	DERMS
Baseline	Disabled	Disabled
DVR-only	Enabled	Disabled
DERMS-only	Disabled	Enabled
DVR + DERMS VPP-only	Enabled	Enabled VPP-only
DVR + DERMS	Enabled	Enabled

TABLE 4. Control enable/disable times.

Control	Enable Time	Disable Time
DVR	16:45	19:05
DERMS voltage regulation	16:40	19:30
DERMS VPP	17:00	19:00

A. BASELINE SCENARIO

The results from the baseline scenario are shown in Fig. 6. The feeder head powers shown in Fig. 6(a) are primarily due to the load demand because the total PV generation shown in Fig. 6(b) is minimal at less than 200 kW. Specifically, the active power demand in phases A, B, and C is nearly 1350 kW, 980 kW, and 930 kW, respectively. The total rated PV capacity is approximately 1600 kW; however, low PV generation is observed during the selected simulation period due to the low solar irradiance level in that period. Because the PV systems are set to operate in unity power factor mode in this scenario, the reactive power generation from the PV is zero.

The LTC and VR tap statuses are shown in Fig. 6(c). The LTC tap position is gradually reduced to −5 during the initial period of the simulation to maintain the feeder head voltage within the deadband around 1.008 p.u. (121 V), which is the LTC local controller voltage regulation set point. The VR tap position gradually increased to 3 during the same period to increase the bus voltages downstream of the VR to keep the VR measured voltages close to the VR initial set point in Table 2.

The range of the bus voltages and the average voltage (Avg. V) during the simulation period are shown in Fig. 6(d). The combined response of the LTC and VR controllers resulted in the voltages falling within a fairly narrow band during the simulation period, as observed from the bus voltages shown in this figure. The voltage dynamics due to the LTC and VR tap changes during the first hour of the simulation can also be observed. It is evident that all the bus voltages are well within the ANSI voltage limits from 0.95 p.u.–1.05 p.u., marked by the dashed red lines in this figure.

The voltage heat map at time 17:00, when the LTC and VR tap positions have settled, is shown in Fig. 7. The bus voltages in the feeder section from the LTC to the VR are lower than those in the feeder section downstream of the VR. Note that this is due to the LTC local controller voltage setting being lower (121 V) than that of the VR (123 V). Although the lowering of the LTC tap position by its respective controller reduced the bus voltages on the feeder up to the VR, the raising of the VR tap position increased the bus voltages downstream of the VR. Because we recorded only the bus voltages from the feeder section modeled in OpenDSS, the subtree section modeled in OPAL-RT is greyed out in this bus voltage heat map and in those presented in the subsequent sections.

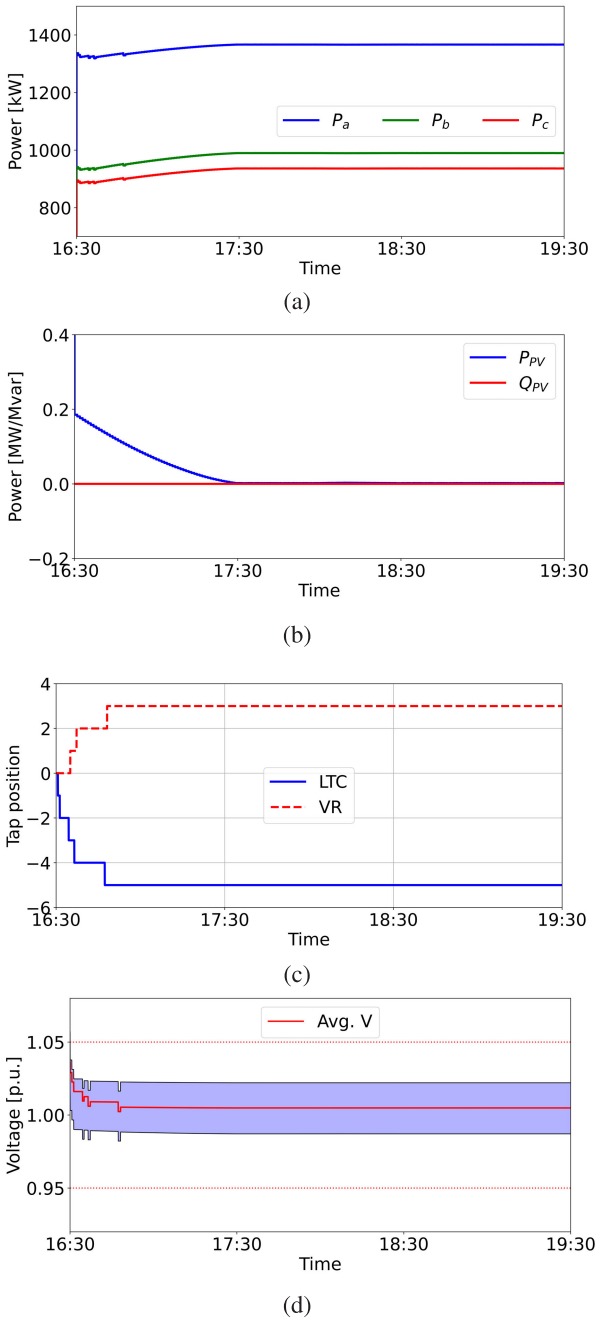

FIGURE 6. Baseline results: (a) feeder head powers, (b) total PV output, (c) LTC and VR tap statuses, and (d) bus voltages.

B. DVR-ONLY SCENARIO

The DVR-only scenario allows us to study the DVR contribution to reducing the peak demand through the CVR. In this scenario, the DVR is enabled at 16:45 and disabled at 19:05, marked by the vertical dashed black lines in Fig. 8. The dynamics in the system due to the

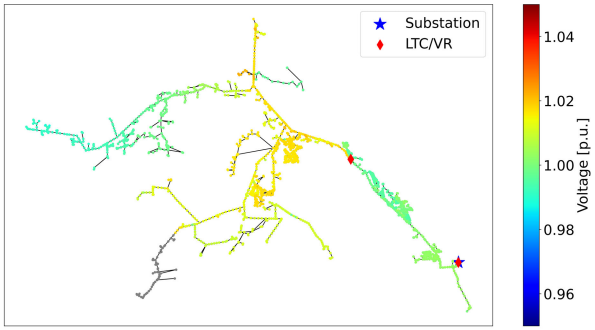

FIGURE 7. Bus voltage heat map at time 17:00 in baseline.

initial conditions are expected to settle within the first 15 minutes, i.e., by 16:45, so we can observe the effect of the DVR more clearly. The legacy device tap changes—i.e., the LTC and VR tap position changes in this scenario—are shown in Fig. 8(a). Before enabling the DVR, the legacy device taps are changed by their respective local controllers. The LTC and VR taps are settled at positions −4 and 2, respectively, at around 16:35 during this period, similar to the baseline scenario. After enabling the DVR application in the ADMS, these taps are changed by the DVR application. The objective of the DVR is to reduce the system voltages as much as possible—without causing voltage exceedances—to accomplish demand reduction; therefore, the DVR gradually lowered the LTC tap position at the feeder head down to −11. Because this would cause low-voltage issues downstream, the DVR raised the VR tap position to 4 to raise the bus voltages far from the substation. The lowering of the LTC tap and the raising of the VR tap positions together help accomplish a flat voltage profile across the feeder.

The bus voltage range is shown in Fig. 8(b). In this figure, the red dotted lines represent the ANSI voltage limits of 0.95 p.u. and 1.05 p.u. As observed in this figure, the bus voltages are restricted to the lower ANSI voltage band from 0.95 p.u.–1.0 p.u. after enabling the DVR; thus, the DVR application effectively performed CVR using the LTC and VR. Some bus voltages went below 0.95 p.u. momentarily at around 16:50 due to the LTC/VR tap position changes.

The DVR application relies on the SCADA voltage measurements from the field as feedback for its algorithm. Up to six downstream voltages can be selected as feedback for each device controlled by the DVR application. This voltage measurement feedback allows the DVR application to detect and mitigate voltage excursions occurring on the feeder. The DVR application compares the feedback measurements with the configured limits (Table 2) and issues set points to the LTC and VR to adjust the voltages to be as low as possible without exceeding the limits. The selected bus voltages sent as the feedback to the DVR for controlling the legacy device taps are shown in Fig. 8(c). It is observed that the feedback voltages are maintained above the DVR lower voltage limit of 0.95 p.u. after the voltage dynamics are settled at around 16:55. The DVR is disabled at 19:05, and therefore the LTC and VR taps went up again based on their local controllers' response. Thus, CVR was not enforced after 19:05.

The feeder head power demand reduction with respect to the baseline is shown in Fig. 8(d). As the DVR reduced the bus voltages, the power demand is reduced through the CVR action. It is observed that power demand is reduced by approximately 100 kW after enabling the DVR when the LTC and VR taps are settled at around 16:50. As the loads are voltage-dependent, the dynamics in the system voltages (Fig. 8(c)) due to the LTC and VR tap changes are reflected in the power demand in Fig. 8(d) between 16:45 and 17:00. Note that in this scenario, the demand reduction is achieved using only the LTC and VR assets, without relying on the BESS.

C. DERMS-ONLY SCENARIO

In this scenario, the DERMS is enabled to perform both the VPP control and the voltage regulation. This is to study the individual contribution of the DERMS in limiting the feeder head powers to the target values while maintaining the bus voltages within the limits without the support of the DVR. The results of this scenario are shown in Fig. 9. The DERMS voltage regulation is enabled at 16:40, and the VPP control is enabled at 17:00, with the target active power limits of 1200 kW, 800 kW, and 800 kW in phases A, B, and C, respectively.

The active powers in the individual phases at the feeder head in this scenario are shown in Fig. 9(a). The powers are similar to those observed in the baseline before the DERMS VPP control is enabled at 17:00. It is evident that the feeder head powers are reduced and limited to the target values after the DERMS VPP is enabled at 17:00. The demand reduction in this scenario is accomplished by DERMS controlling the residential BESS to discharge active power when the VPP control is enabled. The total active power output of the residential BESS and the average SOCs are shown in Fig. 9(b). This is equivalent to the VPP active power because the DERMS does not alter the PV active power for the VPP control. A total of nearly 500 kW is injected into the system in a steady state from 17:30 to 18:40. The VPP control response is fast, and the demand reduction is accomplished within a few minutes (see Fig. 9(a)). As is evident in Fig. 8(b), the total BESS power output remained mostly steady until 18:40. Near 18:40, some of the residential BESS hit their lower SOC limit of 20% and could not inject the required active power into the network. This resulted in the transients in the total BESS power injection and consequently in the feeder head powers, as is evident in Fig. 9(a) and Fig. 9(b).

The total PV power output in this scenario is the same as that in the baseline shown in Fig. 6(b) and is therefore not shown again. The bus voltages shown in Fig. 9(c) are all within the DERMS voltage regulation range from 0.96 p.u.–1.04 p.u.; therefore, the reactive power support from the residential PV is zero. Further, the increase in the bus voltages caused by the active power injection from the BESS when the VPP control is enabled at 17:00 is evident in

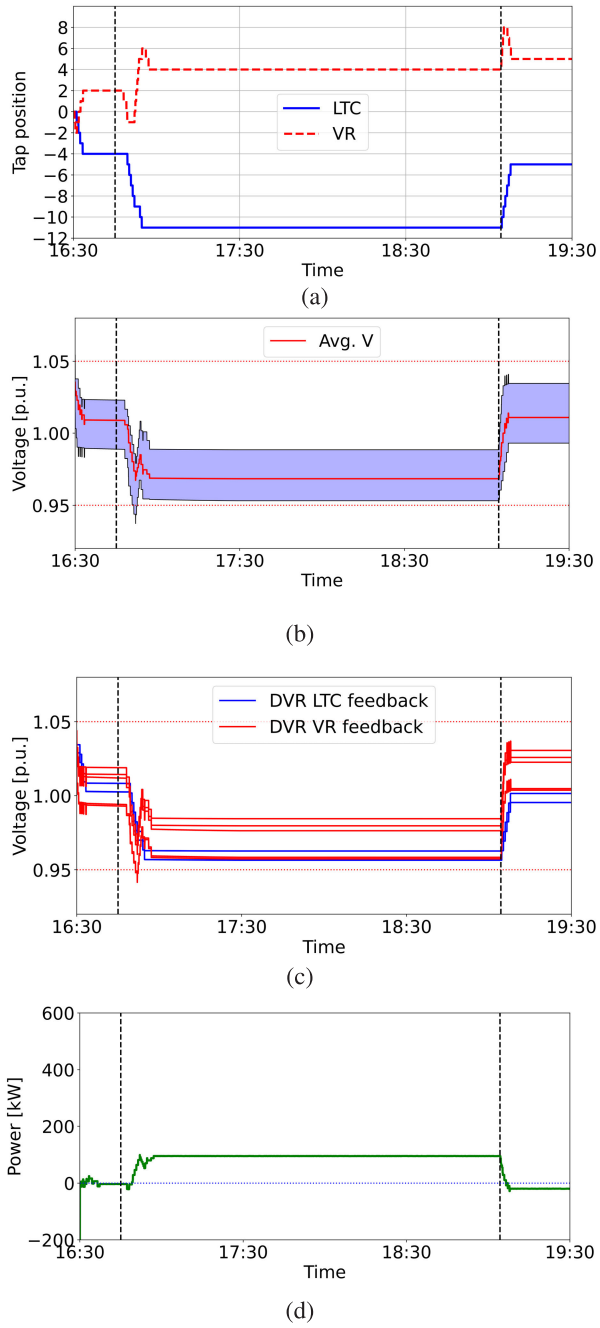

FIGURE 8. DVR-only results: (a) LTC and VR tap statuses, (b) bus voltages, (c) DVR feedback voltages, and (d) feeder head demand reduction.

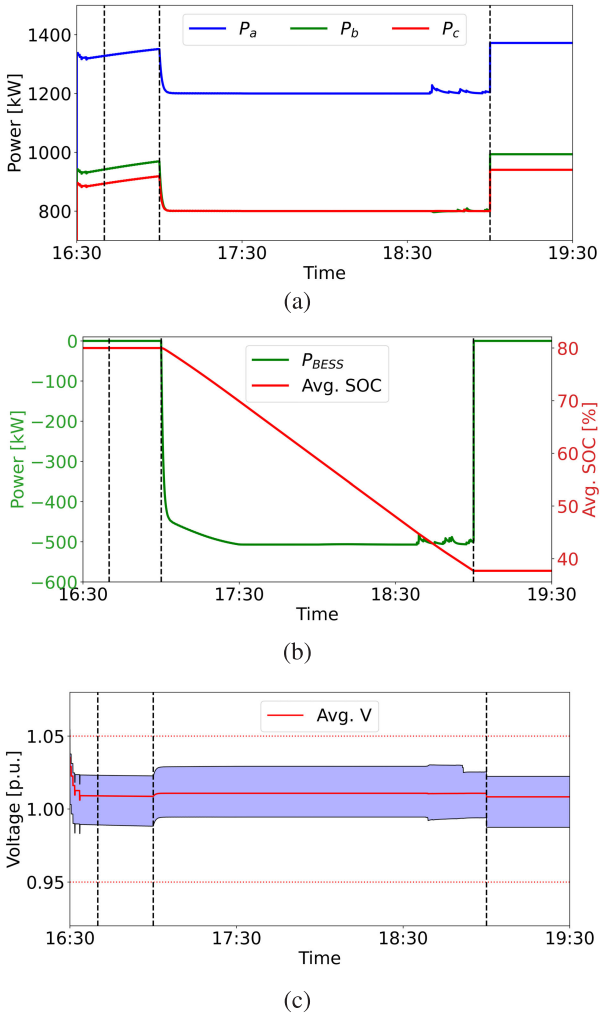

FIGURE 9. DERMS-only results: (a) feeder head power, (b) total storage output and average SOC, and (c) bus voltages.

Fig. 9(c). Some voltage transients are observed around 18:40. This is due to some BESS not being able to discharge the requested powers, as mentioned earlier.

D. DVR + DERMS VPP-ONLY SCENARIO

This real-time simulation is conducted to study the effectiveness of the ADMS using DVR and the DERMS. In this scenario, only VPP control is used by the DERMS without the burden of maintaining the bus voltages within the limits. The total power output and the average SOC of the residential BESS in this scenario are shown in Fig. 10(a). The power output from the BESS in steady state is around 400 kW, which is nearly 100 kW less than that in the DERMS-only scenario. This is because the DVR application in this scenario already reduced the load demand through the CVR by keeping the bus voltages lower than they are in the DERMS-only scenario, as shown in Fig. 9(b). This lower power injection from the BESS ensured that all the BESS had adequate SOC levels until the end of the VPP control period; thus, the BESS power output dynamics observed near 18:40 hours in the DERMS-only scenario are not observed in this scenario. Because the residential BESS discharged the power as requested throughout the VPP control period, the feeder head powers are tightly regulated at their target values, as is evident in Fig. 10(b).

The power output from the individual BESS at 17:30 is shown in Fig. 11 as a heat map. It is observed that most of the active power from the BESS is injected into the two neighborhoods in the middle of the feeder where the DERs are clustered. None of the residential BESS injected more than 5 kW of active power. Although the residential BESS are small and scattered all over the feeder, the DERMS

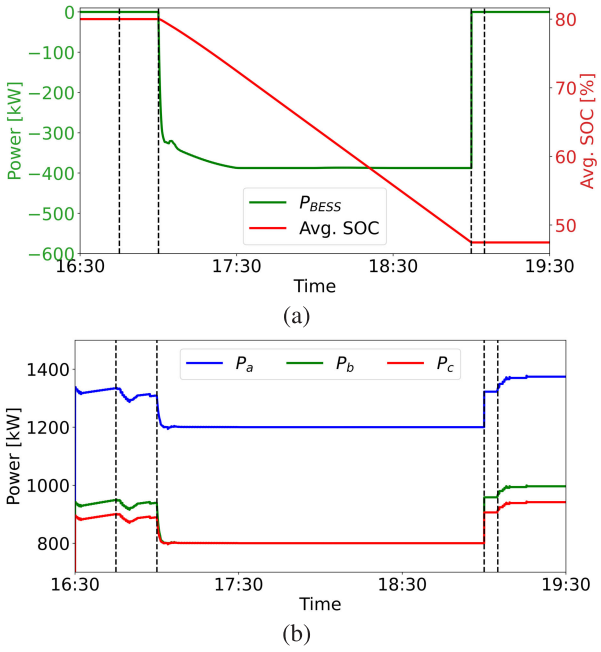

FIGURE 10. DVR + DERMS VPP-only results: (a) total storage output and average SOC and (b) feeder head power.

VPP control successfully obtains the required 400 kW of active power for the peak demand reduction from those BESS.

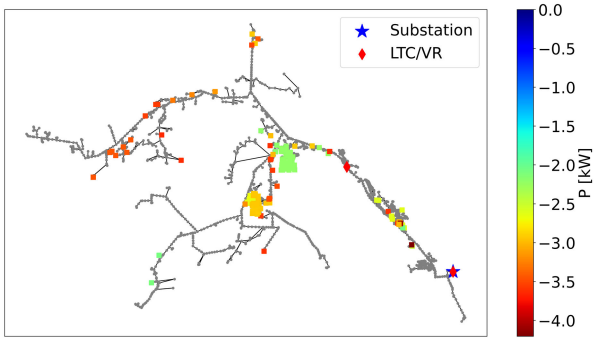

FIGURE 11. Storage output heat map at time 17:30 in the DVR + DERMS VPP-only scenario. A negative sign indicates discharging.

E. DVR + DERMS SCENARIO

In this scenario, the DERMS voltage regulation, DVR, and DERMS VPP controls are all enabled. The feeder head power limit is maintained, and the BESS injection is similar to the DERMS-only scenario; therefore, these results are not shown to avoid redundancy. The bus voltages in this scenario are shown in Fig. 12(a). The bus voltages are all well within the ANSI limits before the DVR is enabled at 16:45. Once enabled, the DVR reduces the bus voltages by controlling the LTC and VR tap positions similar to the DVR-only scenario. This voltage reduction caused some bus voltages to exceed the lower voltage limit of the DERMS voltage regulation (0.96 p.u.), indicated by the dotted green line. The DERMS voltage regulation controlled the PV smart inverters to inject reactive power to increase the bus voltages, as is evident from the total PV output plots in Fig. 12(b). The reactive power output from the PV systems remained mostly constant until the DERMS VPP control was turned off at 19:00. At 19:00, the PV reactive power started increasing as the bus voltages further reduced (see Fig. 12(a)) because of the BESS power injection rapidly dropping to zero. When the DVR was disabled at 19:05, the reactive power from the PV started reducing, finally became zero when the bus voltages increased, and settled within the DERMS voltage regulation limits toward the end of the simulation.

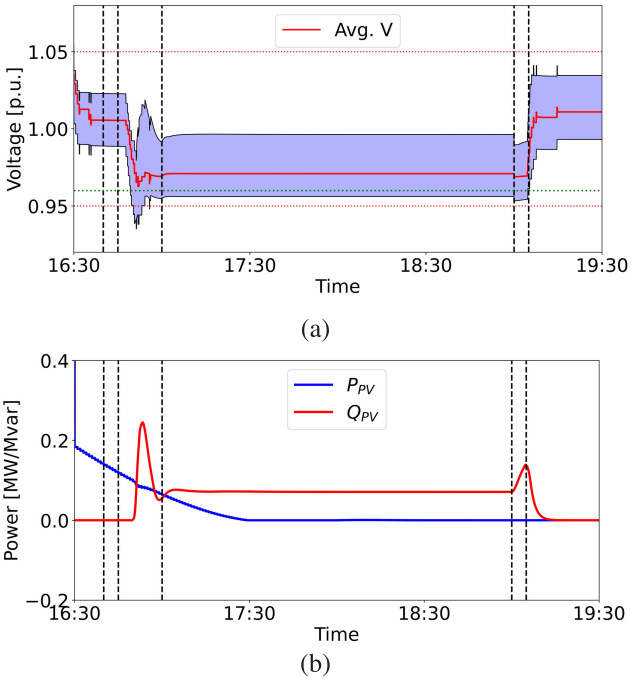

FIGURE 12. DVR + DERMS results: (a) bus voltages and (b) total PV output.

The PV reactive power and bus voltage heat maps are generated from the power flow results at time 17:30 and are shown in Fig. 13. In Fig. 13(a), it is observed that the reactive power injection from the residential PV is primarily concentrated in the two neighborhoods in the middle of the feeder where the DERs are clustered. Consequently, the bus voltages in those neighborhoods are higher than they are in the rest of the feeder, as is evident in Fig. 13(b). Further, the bus voltages in the feeder region between the LTC and VR are lower than the voltages downstream of the VR. This is due to the LTC tap position being considerably lower than the VR tap position. The higher VR tap position and the reactive power support from the PV systems helped maintain the voltages downstream of the VR within the limits.

F. COMPARISON PLOTS

The substation demand reductions with respect to the baseline in different scenarios are compared in Fig. 14(a). It is

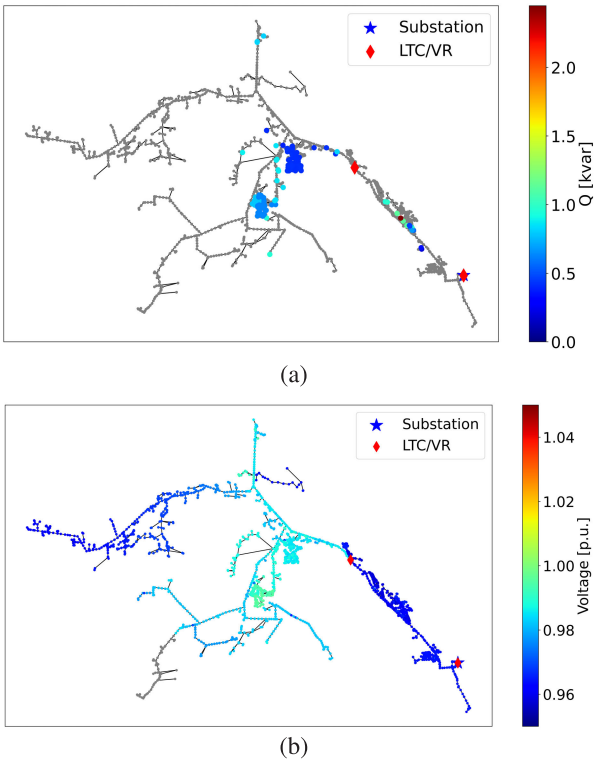

FIGURE 13. DVR + DERMS results at time 17:30: (a) PV reactive power heat map, where a positive sign indicates injection; and (b) bus voltage heat map.

observed that the substation demand reduction is smaller in the DVR-only scenario than in the rest of the scenarios because the load demand reduction in this scenario is achieved by relying on the CVR only. It is observed that a demand reduction of nearly 100 kW is attained using the DVR alone. The DERMS performs the demand reduction through VPP control using the BESS. The active power injection by the BESS has a more direct and significant impact on demand reduction. For the scenarios in which the DERMS is enabled, it is observed that the level of substation demand reduction achieved via the DERMS VPP control of the BESS depends on the total BESS power rating and the power limits set by the ADMS. In the present study, a higher substation demand reduction (approximately 500 kW) is achieved with the DERMS VPP control than can be obtained with the DVR alone because of the availability of sufficient BESS capacity.

The minimum voltage in the feeder in all the scenarios is compared in Fig. 14(b). It is observed that the minimum voltage is lower in the scenarios in which the DVR is enabled than in the other scenarios because the DVR reduced the bus voltages for the CVR. The minimum voltage in the DERMS-only scenario is higher than in the baseline because the active power injection from the BESS caused a voltage increase. The lowest minimum voltage is observed in the DVR + DERMS VPP-only scenario because the DERMS voltage regulation is not activated to maintain the DER bus voltages at the all-electric homes above 0.96 p.u.

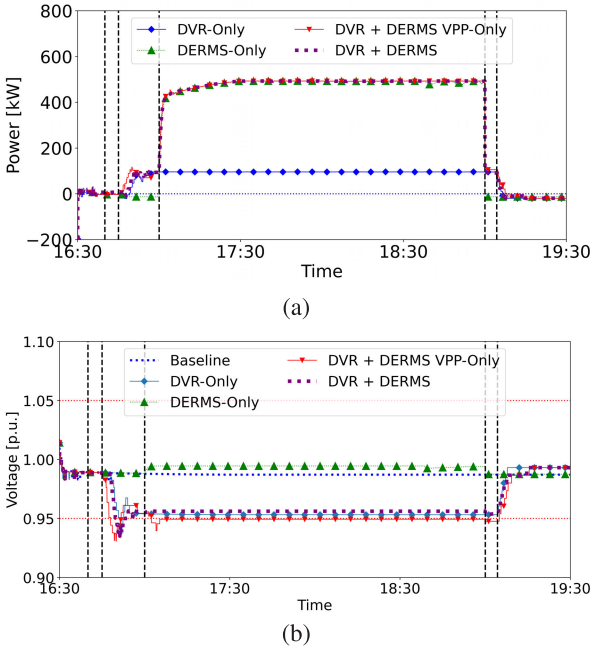

FIGURE 14. Comparison of results: (a) substation demand reduction and (b) minimum voltage.

TABLE 5. Summary of metrics.

Scenario	PR_{max} (kW)	T_{ex} (node-hours)	Q_{max} (kvar)	N_t	ES (%)
Baseline	-	0	0	LTC: 5 VR: 3	-
DVR-only	99.5	1.15	0	LTC: 17 VR: 25	2.09
DERMS-only	493.2	0	0	LTC: 4 VR: 2	9.73*
DVR + DERMS VPP-only	493.3	27.4	0	LTC: 19 VR: 27	10.1*
DVR + DERMS	493.8	3.82	245	LTC: 17 VR: 21	10.06*

*Includes the energy supply from the BESS.

G. METRICS

The metrics described in Section IV are computed for each scenario and are summarized in Table 5. The substation power reduction is higher in the scenarios in which the DERMS VPP is enabled than in the DVR-only scenario. The voltage exceedances are found to be the highest in the DVR + DERMS VPP-only scenario in which the DERMS voltage regulation is disabled. The highest reactive power injection from the PV smart inverters is recorded as 245 kvar in the DVR + DERMS scenario. The LTC and VR tap change counts show that the DVRs extensively used these resources to exercise the CVR. The tap change counts are observed to be considerably high in the scenarios in which the DVR is enabled. The energy savings observed in the DVR-only scenario are 2.09% compared to the baseline. In the other scenarios, the energy savings are nearly 10%. Note that the energy savings values in the table for the scenarios in which the DERMS VPP is enabled include the energy supplied from the BESS.

VI. CONCLUSION AND DISCUSSION

The increasing levels of DERs present both challenges and opportunities for distribution utilities. The advanced grid monitoring and control solutions being deployed by utilities, such as ADMS and DERMS, can help to unlock the benefits of DERs in providing grid services, but because each solution might not have full visibility of the grid assets, interfacing them with each other can provide additional benefits. This paper evaluated the performance of a commercial ADMS interfaced with a prototype DERMS that can manage a VPP—individually and combined—in exercising peak demand reduction while enforcing voltage regulation. Residential PV systems and BESS are considered as the grid resources for the DERMS for the VPP and voltage regulation controls. The results from the CHIL simulations show that both the ADMS and DERMS contribute to peak demand reduction and voltage regulation. The best performance is observed when both the ADMS and DERMS controls are enabled and working cooperatively.

While this work did not include a study of how to ensure cooperation between different control systems, we implemented the following strategies in setting up the simulations when both the ADMS and DERMS were active. We believe that these strategies contributed to the successful cooperation between ADMS and DERMS, which we propose as valuable considerations for similar deployments in the field. First, we staggered the activation (and deactivation) of controls, allowing one control system to settle before the activation of the other. Second, the ADMS and DERMS control different devices, so there is no overlap or conflict of control signals to a specific device. Finally, the ADMS DVR and DERMS applications operate on different time scales, with the DVR application being much slower than the DERMS.

The performance of the ADMS and DERMS controls is evaluated using five metrics. A peak demand reduction of nearly 100 kW is obtained when the ADMS DVR application is acting alone to perform the CVR using the LTC and VR assets. The DERMS VPP control accomplished a peak demand reduction of approximately 500 kW by controlling the residential BESS to discharge power. Substation power deviations from the target values are observed during the VPP control period because some BESS are unable to provide the required powers after hitting their low SOC limits when the DERMS is performing VPP without the ADMS DVR in service. When both the ADMS DVR and DERMS are working together, improved peak demand reduction is accomplished because less power is required from the BESS because some demand reduction is already being achieved by the ADMS DVR application. Some low-voltage exceedances are observed when the ADMS DVR application is enabled because the DVR reduces the bus voltages to perform the CVR. The voltage exceedances are mitigated by the PV reactive power support when the DERMS voltage regulation control is enabled. Higher LTC and VR tap operations are observed in the scenarios where the ADMS DVR is enabled because this application relies on the LTC and VR to perform CVR.

The security issues arising from a coordinated working principle between DERMS and ADMS can be mitigated by implementing robust cybersecurity measures, including access control, vulnerability management, data encryption, supply chain security, and developing a comprehensive incident response plan. Future work will include developing cybersecurity measures for DER communications and extending the prototype DERMS framework to include other DER types such as heat pumps, electric water heaters, and electric vehicles.

ACKNOWLEDGMENT

The authors would like to thank the support and vision of Eric Lightner from the U.S. Department of Energy, in establishing the ADMS Test Bed capability. They also like to thank the support of Jeremy Westbrook from Increase Technologies, who developed the new MultiSpeak business process in partnership with NRECA. The U.S. Government retains and the publisher, by accepting the article for publication, acknowledges that the U.S. Government retains a nonexclusive, paid-up, irrevocable, worldwide license to publish or reproduce the published form of this work, or allow others to do so, for U.S. Government purposes. The authors acknowledge the contributions of Fei Ding, Emiliano Dall'Anese, and Andrey Bernstein in the RT-OPF DERMS algorithm development; Michael Blonsky in the cosimulation development; and Jing Wang in the feeder model development in OPAL-RT.

REFERENCES

[1] *A Vision for the ADMS-DERMS Relationship*. Accessed: Oct. 8, 2021. [Online]. Available: https://cdn2.hubspot.net/hubfs/415845/White%20papers/ADMS-DERMS%20white%20paper/ADMS-DERMS%20whitepaper.pdf

[2] *The National Potential for Load Flexibility*. Accessed: Oct. 8, 2021. [Online]. Available: https://brattlefiles.blob.core.windows.net/files/16639_national_potential_for_load_flexibility_-_final.pdf

[3] B. Kroposki, A. Bernstein, J. King, D. Vaidhynathan, X. Zhou, C.-Y. Chang, and E. Dall'Anese, "Autonomous energy grids: Controlling the future grid with large amounts of distributed energy resources," *IEEE Power Energy Mag.*, vol. 18, no. 6, pp. 37–46, Nov. 2020.

[4] R. A. Walling, R. Saint, R. C. Dugan, J. Burke, and L. A. Kojovic, "Summary of distributed resources impact on power delivery systems," *IEEE Trans. Power Del.*, vol. 23, no. 3, pp. 1636–1644, Jul. 2008.

[5] D. Mcnair, D. Phelan, and L. Coleman, "Voices of experience: Insights into advanced distribution management systems," U.S. Dept. Energy, Washington DC, USA, Tech. Rep., 2015.

[6] L. Strezoski, I. Stefani, and B. Brbaklic, "Active management of distribution systems with high penetration of distributed energy resources," in *Proc. 18th Int. Conf. Smart Technol. (EUROCON)*, Jul. 2019, pp. 1–5.

[7] *A Look Towards the Future Integrating DERMS and ADMS*. Accessed: Oct. 8, 2021. [Online]. Available: https://www.power-grid.com/der-grid-edge/a-look-towards-the-future-integrating-derms-and-adms

[8] N. Petrovic, L. Strezoski, and B. Dumnic, "Overview of software tools for integration and active management of high penetration of DERs in emerging distribution networks," in *Proc.18th Int. Conf. Smart Technol. (EUROCON)*, Jul. 2019, pp. 1–6.

[9] H. Padullaparti, A. Pratt, I. Mendoza, S. Tiwari, M. Baggu, C. Bilby, and Y. Ngo, "Peak load management in distribution systems using legacy utility equipment and distributed energy resources," in *Proc. IEEE Green Technol. Conf. (GreenTech)*, Apr. 2021, pp. 435–441.

[10] H. Saboori, M. Mohammadi, and R. Taghe, "Virtual power plant (VPP), definition, concept, components and types," in *Proc. Asia–Pacific Power Energy Eng. Conf.*, Mar. 2011, pp. 1–4.

[11] S. J. Crocker and J. L. Mathieu, "Adaptive state estimation and control of thermostatic loads for real-time energy balancing," in *Proc. Amer. Control Conf. (ACC)*, Jul. 2016, pp. 3557–3563.

[12] S. P. Meyn, P. Barooah, A. Bušic, Y. Chen, and J. Ehren, "Ancillary service to the grid using intelligent deferrable loads," *IEEE Trans. Autom. Control*, vol. 60, no. 11, pp. 2847–2862, Nov. 2015.

[13] E. Vrettos, F. Oldewurtel, and G. Andersson, "Robust energy-constrained frequency reserves from aggregations of commercial buildings," *IEEE Trans. Power Syst.*, vol. 31, no. 6, pp. 4272–4285, Nov. 2016.

[14] W. Tumin, M. M. Olama, and S. M. Djouadi, "Adaptive control for residential HVAC systems to support grid services," in *Proc. IEEE Power Energy Soc. Innov. Smart Grid Technol. Conf. (ISGT)*, Feb. 2021, pp. 01–05.

[15] P. Munankarmi, X. Jin, F. Ding, and C. Zhao, "Quantification of load flexibility in residential buildings using home energy management systems," in *Proc. Amer. Control Conf. (ACC)*, Jul. 2020, pp. 1311–1316.

[16] C. J. Bay, R. Chintala, V. Chinde, and J. King, "Distributed model predictive control for coordinated, grid-interactive buildings," *Appl. Energy*, vol. 312, Apr. 2022, Art. no. 118612.

[17] R. Ghaemi, A. Kumar, P. Bonanni, and N. Visnevski, "Scalable optimal flexibility control, modeling and estimation of commercial buildings," in *Proc. Amer. Control Conf. (ACC)*, Jul. 2020, pp. 2318–2325.

[18] S. U. Khan, K. K. Mehmood, Z. M. Haider, M. K. Rafique, M. O. Khan, and C.-H. Kim, "Coordination of multiple electric vehicle aggregators for peak shaving and valley filling in distribution feeders," *Energies*, vol. 14, no. 2, p. 352, Jan. 2021.

[19] S. Li, C. Gu, X. Zeng, P. Zhao, X. Pei, and S. Cheng, "Vehicle-to-grid management for multi-time scale grid power balancing," *Energy*, vol. 234, Nov. 2021, Art. no. 121201.

[20] T. Gao, X. Huang, Z. Yang, H. Wang, X. Wen, Q. Zhao, and H. Ding, "A grouping strategy and day-ahead scheduling method of electric vehicles for peak shaving," in *Proc. IEEE 5th Int. Electr. Energy Conf. (CIEEC)*, May 2022, pp. 2676–2681.

[21] K. Sevdari, L. Calearo, S. Striani, P. B. Andersen, M. Marinelli, and L. Rønnow, "Autonomously distributed control of electric vehicle chargers for grid services," in *Proc. IEEE PES Innov. Smart Grid Technol. Eur. (ISGT Europe)*, Oct. 2021, pp. 1–5.

[22] *American National Standard for Electric Power Systems and Equipment-Voltage Ratings (60 Hertz)*, Nat. Elect. Manufacturers Assoc., Rosslyn, VA, USA, 2016.

[23] S. Bolognani, R. Carli, G. Cavraro, and S. Zampieri, "On the need for communication for voltage regulation of power distribution grids," *IEEE Trans. Control Netw. Syst.*, vol. 6, no. 3, pp. 1111–1123, Sep. 2019.

[24] K. Christakou, D.-C. Tomozei, J.-Y. Le Boudec, and M. Paolone, "GECN: Primary voltage control for active distribution networks via real-time demand-response," *IEEE Trans. Smart Grid*, vol. 5, no. 2, pp. 622–631, Mar. 2014.

[25] J. Hu, C. Ye, Y. Ding, J. Tang, and S. Liu, "A distributed MPC to exploit reactive power V2G for real-time voltage regulation in distribution networks," *IEEE Trans. Smart Grid*, vol. 13, no. 1, pp. 576–588, Jan. 2022.

[26] W. Jiao, J. Chen, Q. Wu, C. Li, B. Zhou, and S. Huang, "Distributed coordinated voltage control for distribution networks with DG and OLTC based on MPC and gradient projection," *IEEE Trans. Power Syst.*, vol. 37, no. 1, pp. 680–690, Jan. 2022.

[27] Z. Tang, D. J. Hill, and T. Liu, "Distributed coordinated reactive power control for voltage regulation in distribution networks," *IEEE Trans. Smart Grid*, vol. 12, no. 1, pp. 312–323, Jan. 2021.

[28] P. Yu, C. Wan, Y. Song, and Y. Jiang, "Distributed control of multi-energy storage systems for voltage regulation in distribution networks: A back-and-forth communication framework," *IEEE Trans. Smart Grid*, vol. 12, no. 3, pp. 1964–1977, May 2021.

[29] T. Zhao, A. Parisio, and J. V. Milanović, "Distributed control of battery energy storage systems in distribution networks for voltage regulation at transmission–distribution network interconnection points," *Control Eng. Pract.*, vol. 119, Feb. 2022, Art. no. 104988.

[30] L. Gan and S. H. Low, "An online gradient algorithm for optimal power flow on radial networks," *IEEE J. Sel. Areas Commun.*, vol. 34, no. 3, pp. 625–638, Mar. 2016.

[31] A. Hauswirth, S. Bolognani, G. Hug, and F. Dörfler, "Projected gradient descent on Riemannian manifolds with applications to online power system optimization," in *Proc. 54th Annu. Allerton Conf. Commun., Control, Comput. (Allerton)*, Sep. 2016, pp. 225–232.

[32] A. Hauswirth, A. Zanardi, S. Bolognani, F. Dörfler, and G. Hug, "Online optimization in closed loop on the power flow manifold," in *Proc. IEEE Manchester PowerTech*, Jun. 2017, pp. 1–6.

[33] *Distributed Energy Resources: What's Next for Distribution Grid Management?* Accessed: Jan. 8, 2021. [Online]. Available: https://library.e.abb.com/public/5997220088734d3caddd02d8d3ca49c5/DMS%20and%20DERMS_smartology.pdf?x-sign=MHBC3iLTQMQRFqXJvDDiSeAfIR14JVjP9fkjYT5gG3M3/QJTdI65tx/bNaf4H1BZ

[34] L. Strezoski, H. Padullaparti, F. Ding, and M. Baggu, "Integration of utility distributed energy resource management system and aggregators for evolving distribution system operators," *J. Mod. Power Syst. Clean Energy*, vol. 10, no. 2, pp. 277–285, Mar. 2022.

[35] H. Padullaparti, J. Wang, S. Veda, M. Baggu, and A. Golnas, "Evaluation of data-enhanced hierarchical control for distribution feeders with high PV penetration," *IEEE Access*, vol. 10, pp. 42860–42872, 2022.

[36] J. Wang, H. Padullaparti, F. Ding, M. Baggu, and M. Symko-Davies, "Voltage regulation performance evaluation of distributed energy resource management via advanced hardware-in-the-loop simulation," *Energies*, vol. 14, no. 20, p. 6734, Oct. 2021.

[37] J. Wang, M. Blonsky, F. Ding, S. C. Drew, H. Padullaparti, S. Ghosh, I. Mendoza, S. Tiwari, J. E. Martinez, J. J. D. Dahdah, F. A. M. Bazzani, M. Baggu, M. Symko-Davies, C. Bilby, and B. Hannegan, "Performance evaluation of distributed energy resource management via advanced hardware-in-the-loop simulation," in *Proc. IEEE Power Energy Soc. Innov. Smart Grid Technol. Conf. (ISGT)*, Feb. 2020, pp. 1–5.

[38] J. Wang, H. Padullaparti, S. Veda, I. Mendoza, S. Tiwari, and M. Baggu, "Performance evaluation of data-enhanced hierarchical control for grid operations," in *Proc. IEEE Power Energy Soc. Gen. Meeting (PESGM)*, Aug. 2020, pp. 1–5.

[39] *Dynamic Voltage Regulation (DVR)*. Accessed: Jul. 10, 2021. [Online]. Available: https://www.survalent.com/wp-content/uploads/resource/Survalent_Dynamic-Voltage-Regulation-DVR-Brochure.pdf

[40] E. Dall'Anese and A. Simonetto, "Optimal power flow pursuit," *IEEE Trans. Smart Grid*, vol. 9, no. 2, pp. 942–952, Mar. 2018.

[41] *How Net Metering Works*. Accessed: Dec. 8, 2023. [Online]. Available: https://www.holycross.com/solar-rates/

[42] M. S. Hossan and B. H. Chowdhury, "Exponential factor dependent ZIP coefficients extraction and impacts of CVR in a utility feeder," in *Proc. North Amer. Power Symp. (NAPS)*, Oct. 2015, pp. 1–6.

[43] D. Jager and A. Andreas, "NREL national wind technology center (NWTC): M2 tower; Boulder, Colorado (data)," Nat. Renew. Energy Lab. (NREL), Golden, CO, USA, Tech. Rep. NREL/DA-5500-56489, 1996.

[44] P. Paudyal, F. Ding, S. Ghosh, M. Baggu, M. Symko-Davies, C. Bilby, and B. Hannegan, "The impact of behind-the-meter heterogeneous distributed energy resources on distribution grids," in *Proc. 47th IEEE Photovolt. Spec. Conf. (PVSC)*, Jun. 2020, pp. 857–862.

[45] A. Pratt, M. Baggu, F. Ding, S. Veda, I. Mendoza, and E. Lightner, "A test bed to evaluate advanced distribution management systems for modern power systems," in *Proc. IEEE 18th Int. Conf. Smart Technol. (EUROCON)*, Jul. 2019, pp. 1–6.

[46] E. Dall'Anese, S. S. Guggilam, A. Simonetto, Y. C. Chen, and S. V. Dhople, "Optimal regulation of virtual power plants," *IEEE Trans. Power Syst.*, vol. 33, no. 2, pp. 1868–1881, Mar. 2018.

[47] F. Ding, "Distributed energy resource management solution using real-time optimization," NREL Softw. Record, Golden, CO, USA, Tech. Rep. SWR-20-46, 2019.

[48] *MultiSpeak*. Accessed: Jan. 8, 2021. [Online]. Available: https://www.multispeak.org/

[49] B. Palmintier, D. Krishnamurthy, P. Top, S. Smith, J. Daily, and J. Fuller, "Design of the HELICS high-performance transmission-distribution-communication-market co-simulation framework," in *Proc. Workshop Modeling Simulation Cyber-Phys. Energy Syst. (MSCPES)*, Apr. 2017, pp. 1–6.

[50] M. Blonsky, H. Padullaparti, F. Ding, and S. Veda, "Distribution system co-simulator with distributed energy resource controls," NREL Softw. Rec., Tech. Rep. SWR-21-74, 2021.

HARSHA PADULLAPARTI (Senior Member, IEEE) received the B.Tech. degree in electrical and electronics engineering from Jawaharlal Nehru Technological University Hyderabad, Hyderabad, India, in 2007, the M.S. degree in electrical engineering from the Indian Institute of Technology Madras, India, in 2010, and the Ph.D. degree in electrical and computer engineering from the University of Texas at Austin, in 2018. He was a Senior Engineer with Power Grid Corporation of India Ltd. (PGCIL), from 2009 to 2014. He is currently a Senior Researcher with the Power Systems Engineering Center, National Renewable Energy Laboratory, Golden, CO, USA. His research interests include data analytics for distribution grid operations, advanced distribution management systems, distributed energy resources management systems, distribution system modeling, and renewable energy integration.

ANNABELLE PRATT (Senior Member, IEEE) received the bachelor's and master's degrees in electrical and electronic engineering from Stellenbosch University, South Africa, and the Ph.D. degree in electrical engineering from Oregon State University. She is currently a Chief Engineer with the National Renewable Energy Laboratory (NREL), where she involved on distribution management systems and microgrids, and the application of power and controller-hardware-in-the-loop techniques to system performance evaluation. Prior to joining NREL, she was a Senior Power Research Engineer with Intel Labs, and previously she was with Advanced Energy Industries, where she developed power supplies for the semiconductor manufacturing and architectural glass coating industries.

ISMAEL MENDOZA (Member, IEEE) received the Bachelor of Science degree in electrical engineering from the Colorado School of Mines, Golden, CO, USA, in 2003. He is currently a Senior Engineer with the National Renewable Energy Laboratory, Golden. His research interests include the integration of controller-hardware-in-the-loop and power-hardware-in-the-loop to power model interactions with advanced distribution management systems for energy management, system resilience, and interoperability in distribution and microgrid networks.

SOUMYA TIWARI (Member, IEEE) received the Bachelor of Engineering degree in electronics and instrumentation engineering from Rajiv Gandhi Technical University, Bhopal, India, in 2012, and the Master of Science degree in electrical engineering from San Diego State University, in 2016. She was a Research Engineer with the Energy Systems Integration Facility Operation's Engineering Group, National Renewable Energy Laboratory, Golden, CO, USA, where she contributed to this work. She is currently the Manager of Toronto Hydro, Canada. Her research interests include distribution and transmission system modeling and controls on digital real-time simulators and the integration of controller- and power-hardware-in-the-loop systems for overall performance evaluation.

MURALI BAGGU (Senior Member, IEEE) received the B.Tech. degree in electrical and electronics engineering from Kakatiya University, India, the M.S. degree in electrical engineering from the University of Idaho, Moscow, ID, USA, and the Ph.D. degree in electrical engineering from the Missouri University of Science and Technology, Rolla, MO, USA, in 2009.

He is currently the Laboratory Program Manager of Grid Integration, National Renewable Energy Laboratory (NREL), Golden, CO, USA. In this role, he leads the DOE Office of Electricity and Grid Modernization Initiative programs, NREL. He also directs and leads NREL's Advanced Distribution Management System and Puerto Rico Grid Recovery and Resilience efforts. He has extensive experience in advanced grid control and evaluation for future power systems with high penetrations of distributed energy resources. Before joining NREL, he was a Lead Power Systems Engineer with GE Global Research, Niskayuna, NY, USA, where he developed advanced volt/VAR control and distributed energy resource management algorithms. At GE Global Research, he led the technology development and deployment of large-scale energy storage integration with photovoltaic systems for the U.S. Department of Defense Marine Corps Installations. He has four issued patents and more than 50 publications in these areas. His research interests include the grid integration of renewable systems (wind and PV), energy storage system integration, distribution automation, and grid operations and control.

Dr. Baggu is the Chair of the IEEE Distribution System Operation and Planning Subcommittee.

CHRIS BILBY (Member, IEEE) received the bachelor's degree in mechanical engineering from The University of Oklahoma, in 2002. He was a Research Engineer with Holy Cross Energy (HCE), a rural electric cooperative with headquarters in Glenwood Springs, CO, USA, where he contributed to this work. He is currently a Senior Engineer with Stem, Inc. He supported the HCE's Engineering Department by studying and planning for the increasing number of distributed energy resources and their effects on system loading, reliability, and load profiles. He has authored HCE's electrification of transportation strategy and was the Technical Lead of HCE's programs and microgrid developments. He holds patents in solar array support methods and the processing of complex composite geometric structures.

YOUNG NGO (Member, IEEE) received the bachelor's and Master of Science degrees in electrical engineering from the Stevens Institute of Technology, Hoboken, NJ, USA, and the EMBA degree in marketing and finance from Columbia University, New York.

He is currently the Chief Technology Officer of Survalent Technology Corporation, an industry-leading provider of operational software solutions for electrical distribution utilities. He is responsible for company's technology and product vision, strategy, and roadmap. Prior to Survalent Technology Corporation, he was the President and the CEO of Kinects Solutions, the General Manager of Kinectrics, and the Business Director of Honeywell.